# Statistical fluctuations in HfO$_x$ resistive-switching memory (RRAM): Part I - Set/Reset variability

S. Ambrogio, *Student Member, IEEE*, S. Balatti, *Student Member, IEEE*, A. Cubeta, *Student Member, IEEE*,
A. Calderoni, N. Ramaswamy, *Senior Member, IEEE*, D. Ielmini, *Senior Member, IEEE*

*Abstract*—**Resistive switching memory (RRAM) relies on the voltage-driven formation/disruption of a conductive filament (CF) across a thin insulating layer. Due to the 1D structure of the CF and the discrete nature of defects, the set and reset states of the memory device generally display statistical variability from cycle to cycle. For projecting cell downscaling and designing improved programming operations, the variability as a function of the operation parameters, such as the maximum current in the set process and the maximum voltage in the reset process, need to be evaluated and understood. This work addresses set/reset variability, presenting statistical data for HfO$_x$-based RRAM and introducing a physics-based Monte Carlo model for switching statistics. The model can predict the distribution of the set state as a function of the compliance (maximum) current during set and the distribution of the reset state as a function of the stop (maximum) voltage during reset. Numerical modeling results are finally presented to provide additional insight into discrete fluctuation events.**

**Keywords: resistive switching memory (RRAM), noise fluctuations, random telegraph noise.**

## I. INTRODUCTION

The resistive switching memory (RRAM) is a two-terminal resistive memory, where different resistance states can be achieved by the formation and the disconnection of a conductive filament (CF) through an insulating layer, typically a transition metal oxide [1]. RRAM shows fast switching [2] and low power consumption, thanks to the ability to control the size of the CF through the compliance current $I_C$ during the set operation [3], [4]. As the CF approaches the few-atom size, however, RRAM becomes vulnerable to variability and fluctuation effects, such as the switching statistics [5]–[10] and noise [11]–[14]. Given the relatively small resistance window of oxide-based RRAM, read/program fluctuations can significantly affect the scalability and the low-current operation [15]. To assess the scalability of RRAM and to introduce adequate programming algorithms with controlled variability, the switching statistics must be understood through experiments and physics-based models.

This work addresses statistical variability of set and reset operations in oxide-based bipolar RRAM [16]. First, an analytical model for set and reset processes is proposed, based
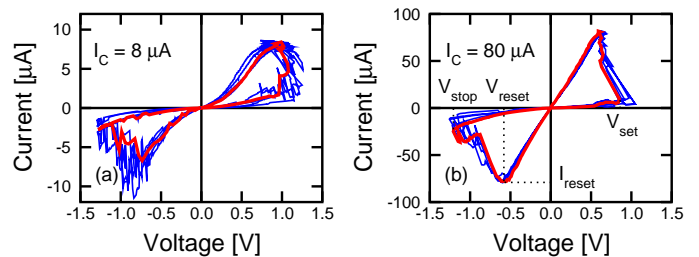
Fig. 1. Measured *I-V* curves for $I_C$ = 8 $\mu$A (a) and 80 $\mu$A (b). In both figures, a typical *I-V* curve (thick line) and repeated measurements on different cycles (thin line) are shown to highlight the variability of the switching parameters. The set voltage $V_{set}$, the reset voltage $V_{reset}$, the reset current $I_{reset}$ and the stop voltage $V_{stop}$ are also shown.

on previous simulation results by a numerical model of ion migration by thermally-activated drift and diffusion [17]. A Monte Carlo model for stochastic set/reset processes is then developed by extending the analytical switching model to a distribution of energy barriers for ion migration. The model is applied to study the dependence of the set state distribution on the compliance current $I_C$, namely the maximum current during set operation, controlling the size of the CF. It is found that the relative spread of set state parameters, such as the resistance, increases for decreasing $I_C$, due to the discrete migration events controlling CF connection [7,15]. The statistical variability of the reset state is then addressed, discussing the dependence on $I_C$ and on the maximum voltage $V_{stop}$ along the reset sweep. A preliminary study on variability modeling was previously reported in [16]. In this work, we extend the analysis of [16] by reporting the variability of reset parameters, *i.e.*, reset voltage and current, the reset-state variability as a function of $I_C$ and a numerical model for reset variability through a new energy landscape approach. The statistical model for read noise, namely random telegraph noise (RTN), will be addressed in the companion paper [18].

## II. EXPERIMENTAL SAMPLES AND CHARACTERISTICS

Experiments were performed on RRAM devices in series with a MOS transistor to accurately control the maximum current flowing in the device and the resistance in the set state [3], [4]. The RRAM device consists of a HfO$_2$ layer sandwiched between two TiN electrodes. A Ti cap was interposed between the top TiN electrode and HfO$_2$ to getter oxygen and form a local substoichiometric HfO$_x$ (x < 2) layer close to the top electrode. The HfO$_2$ layer had a thickness of 10 nm and was amorphous after deposition. The Ti cap thickness was 15 nm.
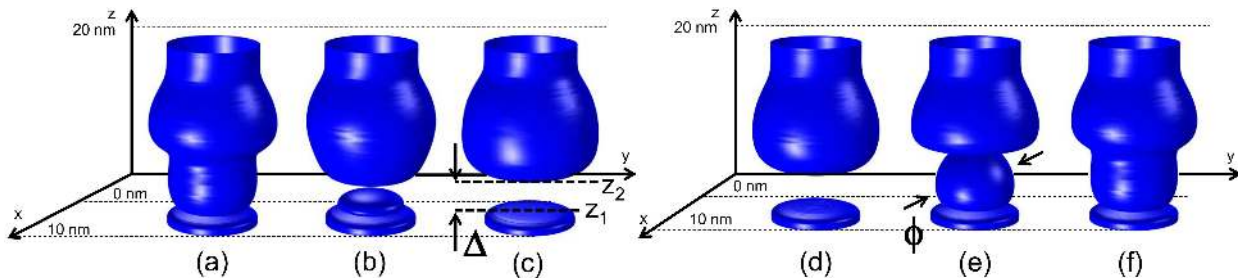
Fig. 2. Contour plots of the calculated defect concentration for a reset transition (a, b, c) and a set transition (d, e, f). The defect concentration was calculated by a numerical model for set/reset processes due to ion migration. The gap length $\Delta$ increases during the reset transition, while the CF diameter $\phi$ in the gap region increases during set transition.

Fig. 1 shows typical current-voltage ($I$-$V$) characteristics obtained at different cycles with compliance current $I_C = 8$ $\mu$A (a) and $I_C = 80$ $\mu$A (b). The voltage drop across the MOSFET was subtracted to provide the switching characteristics of the device only. The set transition takes place at a positive voltage $V_{set}$, while the onset of the reset transition can be seen at a negative voltage $V_{reset}$ and current $I_{reset}$, as indicated in Fig. 1b. The negative sweep is generally completed at a negative voltage $V_{stop}$, which is necessary to achieve the high resistance of the reset state [3], [19], [20]. The current compliance $I_C$ controls the resistance $R$ in the set state and $I_{reset}$, thus plays an essential role in limiting the power consumption in the memory cell [2], [3], [21]. The $I$-$V$ characteristics show a variability from cycle to cycle, which increases for decreasing $I_C$.

III. ANALYTICAL SET/RESET MODEL

The set and reset transitions can be described as the change of shape and size of the CF resulting from the migration of ionized defects, such as oxygen vacancies and excess metal atoms. A numerical model based on temperature- and field-accelerated ionic drift-diffusion was recently reported [17]. Fig. 2 shows numerical simulation results for the contour plot of the defect density during reset transition (a, b, c) and set transition (d, e, f). Simulation results were obtained assuming a thickness of 20 nm for the HfO$_x$ switching layer and a CF diameter around 5 nm. Starting from a continuous conductive filament (Fig. 2a), the reset transition results in the gradual opening of a depleted gap due to the ion migration toward the negatively-biased top electrode (Fig. 2b and c). The depleted gap has a high resistivity, therefore can account for the resistance increase during reset.

To analytically describe the reset transition, the growth rate of the gap length $\Delta$ can be written as:

$$\frac{d\Delta}{dt} = Ae^{-\frac{E_A - \alpha qV}{kT}}, \quad (1)$$

where $A$ is a pre-exponential coefficient [ms$^{-1}$], $E_A$ is the energy barrier for ion migration, $\alpha$ is a barrier lowering coefficient, $V$ is the voltage drop across the gap, $k$ is the Boltzmann constant and $T$ is the local temperature at the injecting edge $z_1$ (see Fig. 2c). Eq. (1) relies on reset transition being controlled by ion hopping which is a thermally activated process with energy barrier $E_A$ [22], [23]. The latter might
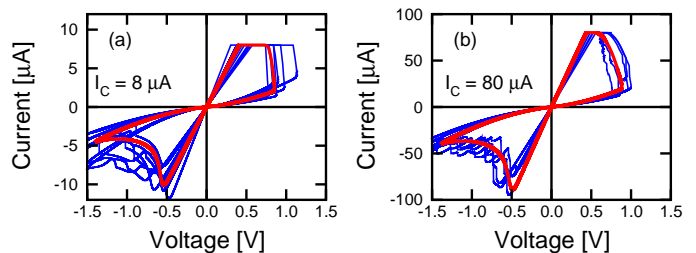


Fig. 3. Calculated $I$-$V$ curves obtained by the analytical model (thick line) and repeated $I$-$V$ curves obtained by the Monte Carlo variability model (thin line) for $I_C = 8$ $\mu$A (a) and 80 $\mu$A (b). The statistical fluctuation of resistance, switching current and switching voltage increases for decreasing $I_C$.
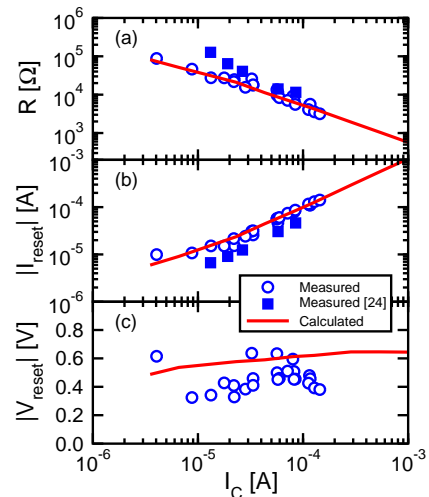


Fig. 4. Average of measured and calculated set state resistance $R$ (a), reset current $I_{reset}$ (b) and reset voltage $V_{reset}$ (c) as a function of $I_C$. The absolute values of current and voltage are reported. The average values were obtained over 50 cycles at each $I_C$. Resistance (a) and $V_{reset}$ (b) are corrected by the voltage drop across the select MOSFET in the 1T1R structure. Data for HfO$_x$ RRAM samples from [24] are also reported for comparison.

also include the energy barrier for defect ionization, which is necessary for migration since only ionized defects can respond to the electric field. It is thus assumed that the gap depletion rate increases proportional to the defect migration velocity, described by the Arrhenius law in Eq. (1).

Starting from the reset state in Fig. 2d (same as the final state in Fig. 2c), the set transition causes defect migration

toward the bottom electrode as a result of the positive voltage applied to the top electrode. Defects are therefore injected into the gap leading to an increase of defect concentration which appears as an increase of CF diameter $\phi$ within the gap region (Fig. 2e and f). Defect migration is sustained by the CF reservoir at the top electrode side. Similar to Eq. (1), we can therefore describe the diameter growth rate by:

$$\frac{d\phi}{dt} = Ae^{-\frac{E_A - \alpha qV}{kT}}, \qquad (2)$$

where the same parameters as in Eq. (1) were used, except for $T$ which is now evaluated at the injecting top boundary at $z_2$. The same coefficient $A$ as Eq. (1) was used in Eq. (2) for simplicity. Note that, in our model, migration mostly takes place between top/bottom reservoir of defects and the gap region, with no interaction with the electrodes. This approximation might be acceptable, given the low temperature and low electric field at the electrodes, compared to the active part of the CF in the gap or bottleneck region. In the analytical model we also neglected the radial diffusion of ions, driven by the defect concentration gradient, in favor of vertical migration driven by the field. This might be understood by the barrier lowering along the field direction [25], which makes field-driven migration the dominant microscopic process during bipolar switching.

The resistance $R$ of the device was calculated as the series of three CF regions, namely (i) a stub at the top-electrode side, (ii) a gap region and (iii) a stub at the bottom electrode side. The two stubs were assumed to have a fixed diameter, dictated by $I_C$ during the forming operation. The gap region was assumed to have length $\Delta$, dictated by the reset operation, and a filament diameter $\phi$, dictated by the set operation. This allowed for the calculation of the CF resistance during any set/reset process. The I-V curves were calculated by simulating a voltage increase with ramp rate dV/dt = 1 Vs$^{-1}$ applied to the device and calculating the consequent change of resistance through Eqs. (1) and (2). Fig. 3 shows the $I$-$V$ characteristics, thick line, obtained by the analytical model for $I_C = 8$ $\mu$A (a) and $I_C = 80$ $\mu$A (b). In the model, $I_C$ controls the set state $R$ and $I_{reset}$, similar to experimental results in Fig. 1. This is further confirmed in Fig. 4, showing measured and calculated $R$ for the set state (a), $I_{reset}$ (b) and $V_{reset}$ (c) as a function of $I_C$. The reset voltage was extracted in correspondence of the maximum current $I_{reset}$ along the negative voltage sweep, in both experiments and calculations. Experimental results were obtained as the median value over a statistics of 50 cycles for the same RRAM device. Data for HfO$_x$ RRAM samples from [24] are also reported for comparison. Calculations were obtained for $E_A = 1.2$ eV, $\alpha = 0.05$ and $A = 300$ ms$^{-1}$. The resistance decreases at increasing $I_C$ as a result of the larger diameter $\phi$ achieved during set transition [25]. The product of $R$ and $I_C$ is approximately constant and equal to $V_C \approx 0.5$ V, which describes the voltage needed to activate ion migration in the timescale of the experiment (about 1 s in this work) [25]. In fact, the voltage across the device decreases due to CF growth at a constant $I_C$, therefore the growth process stops when the voltage equals the critical value $V_C$ for ion migration. The reset current $I_{reset}$ increases according to
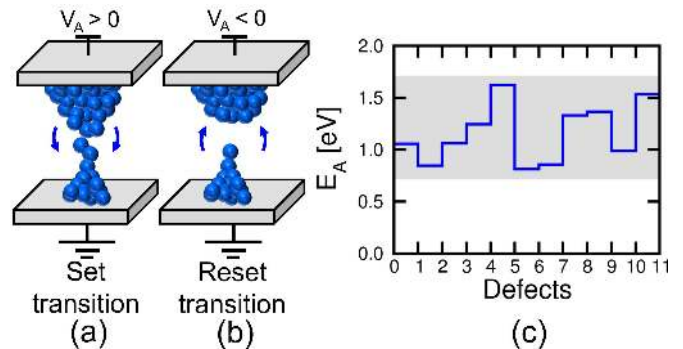


Fig. 5. Schematic illustration of the discrete defect migration in the Monte Carlo model for variability. Set transition is described as the migration of discrete defects, resulting in the CF diameter growth (a) while reset transition is described as the migration of discrete defects, resulting in the gap length increase (b). Energy barriers for the injection of individual defects, or defect clusters, are randomly extracted within a uniform distribution between 0.7 eV and 1.7 eV (c).

$I_{reset} \approx I_C$ in Fig. 4b, while $V_{reset}$ is approximately constant in Fig. 4c [26]. Calculated results from the analytical model show good agreement with data, supporting our analytical model for set/reset processes.

## IV. MONTE CARLO MODEL

To account for switching variability in Fig. 1, random migration of discrete defects was introduced in the analytical model by a Monte Carlo approach. Fig. 5 shows a schematic for the discrete migration of ionized defects during set transition (a) and reset transition (b). In the Monte Carlo model, each defect (or defect cluster) has a characteristic energy barrier $E_A$ describing its hopping mobility. The CF or gap growths therefore follow a sequence of discrete defect events, each characterized by a random value of $E_A$ and a corresponding migration rate. The energy barrier was randomly generated from a uniform distribution between 0.7 and 1.7 eV, which is centered around the average value of 1.2 eV used in the calculations of Figs. 3 and 4. A uniform distribution was used instead of a normal distribution, since it allows for better agreement with statistical variability data. The random $E_A$ was used in the continuous Eqs. (1) and (2), where the stochastic migration time of each individual defect for a given $E_A$ was neglected compared to the large variability of time deriving from the spread of $E_A$ in Fig. 5c. The random $E_A$ allows to describe the structural change of the HfO$_x$ material in the gap region, due to change of the composition profile resulting from the growth of the CF during set transition and the growth of a depleted gap during reset transition. As a result, the structure of the migration channel changes with time during the transition, resulting in a random change of the energy barrier for defect migration. A constant volume of 0.6 nm$^3$, corresponding to about 13 point defects in HfO$_x$, was attributed to each defect cluster with a certain value of $E_A$. The value of $E_A$ was updated by a new random generation as the migration of a whole cluster of 13 defects was completed according to (1) or (2). As an example, Fig. 5c shows the randomly generated $E_A$ for 11 groups of defects during a set transition calculated by the Monte Carlo model.
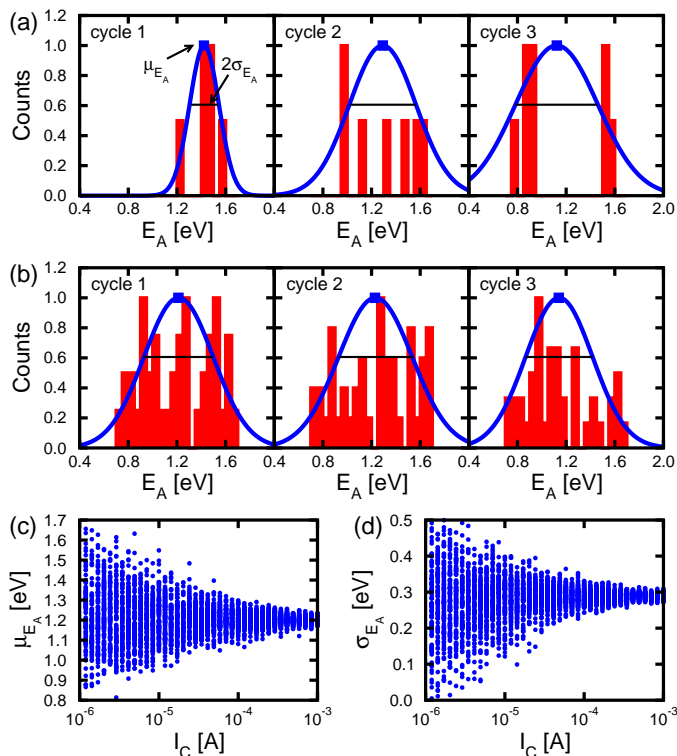
Fig. 6. Distributions of $E_A$ for three set/reset cycles and the corresponding gaussian fits obtained from the Monte Carlo model for $I_C = 8$ $\mu$A (a) and 80 $\mu$A (b). Both the average value $\mu_{E_A}$ and the standard deviation $\sigma_{E_A}$ display more fluctuation from cycle to cycle in the case of $I_C = 8$ $\mu$A, as summarized by $\mu_{E_A}$ (c) and $\sigma_{E_A}$ (d) as a function of $I_C$.

## V. SIMULATION RESULTS

Fig. 3 shows typical $I$-$V$ characteristics (thin line), obtained by the Monte Carlo model for $I_C = 8$ $\mu$A (a) and $I_C = 80$ $\mu$A (b). Random migration events appear as step changes of resistance during both set and reset transitions. Most importantly, random defect migration induces cycle-to-cycle variations of switching parameters, such as $R$ of the set and reset states, $V_{set}$, $V_{reset}$ and $I_{reset}$, similar to the experimental characteristics in Fig. 1. The switching variability is significantly higher for $I_C = 8$ $\mu$A as compared to $I_C = 80$ $\mu$A, similar to the experimental data in Fig. 1. The enhanced statistical fluctuation at decreasing $I_C$ is explained in Fig. 6, showing the histograms of the generated $E_A$ associated to each defect cluster contributing to set/reset processes along 3 $I$-$V$ cycles at $I_C = 8$ $\mu$A (a) and $I_C = 80$ $\mu$A (b). The gaussian fitting curve is also shown for each histogram: the average value $\mu_{E_A}$ and the standard deviation $\sigma_{E_A}$ of the $E_A$ distribution change from cycle to cycle for $I_C = 8$ $\mu$A in Fig. 6a, as a result of the small number of injection events. On the other hand, the Gaussian distributions are highly stable in terms of $\mu_{E_A}$ and $\sigma_{E_A}$ for $I_C = 80$ $\mu$A in Fig. 6b, thanks to the large number of defects involved in the set/reset transitions. To further highlight the dependence on $I_C$, Fig. 6 also shows $\mu_{E_A}$ (c) and $\sigma_{E_A}$ (d) of individual $I$-$V$ curves as a function of $I_C$. As $I_C$ increases, the distributions of both $\mu_{E_A}$ and $\sigma_{E_A}$ become narrower, indicating the decrease of the cycle-to-cycle variations for increasing size of the CF. Clearly, the large
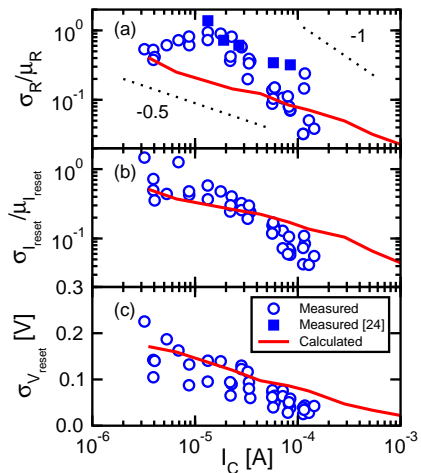


Fig. 7. Relative spread of set state resistance $\sigma_R/\mu_R$ (a), relative spread of $I_{reset}$ (b) and standard deviation of $V_{reset}$ (c) as a function of $I_C$, from both data and calculations. Data were collected from a statistics of 50 cycles for a single 1T1R structure. Data for HfO$_x$ RRAM samples from [24] are also reported for comparison.

fluctuation of $E_A$ at small $I_C$ clearly results in the enhanced switching variability in Fig. 3a.

### A. Set state variability as a function of $I_C$

To highlight the $I_C$-dependence of switching variability, Fig. 7a shows the relative spread of $R$ for the set state as a function of $I_C$. The relative spread was evaluated for both data and calculations as the ratio between the standard deviation $\sigma_R$ and the median value $\mu_R$ of the distribution of $R$ over 50 cycles on the same device. Both data and calculations show a decrease of $\sigma_R/\mu_R$ for increasing $I_C$, due to the averaging effect of discrete ion migration in large CFs. Similar behaviors are found for the relative spread of the reset current $\sigma_{I_{reset}}/\mu_{I_{reset}}$ in Fig. 7b and for the standard deviation $\sigma_{V_{reset}}$ of the reset voltage in Fig. 7c. The calculated relative spread of the resistance in Fig. 7a shows a slope of -0.5, which is consistent with the Poisson statistics that controls the number of defects in the CF after set transition [7]. However, the experimental data show a larger slope of about -1, which can be interpreted by the additional contribution of random position of defects, as schematically shown in Fig. 8. In fact, our model only accounts for the variable number of injected defects as a result of the random $E_A$, while defect position within the gap region is not considered. Fig. 8 schematically shows a CF with only 4 defects A, B, C, D in the gap region. The position of these defects is randomly changed from cycle to cycle, e.g., the defects can be located at the top electrode side (a), at the bottom electrode side (b) or evenly distributed (c). Depending on the local defect arrangement, different band structures and transport properties are obtained, thus resulting in different values of the set state $R$. This additional variability source might account for the slope in Fig. 7a being higher than the theoretical value of 0.5 at least in the range of relatively low $I_C$. More studies are needed to clarify the relatively high slope of $\sigma_R/R$ also in the high $I_C$ regime.
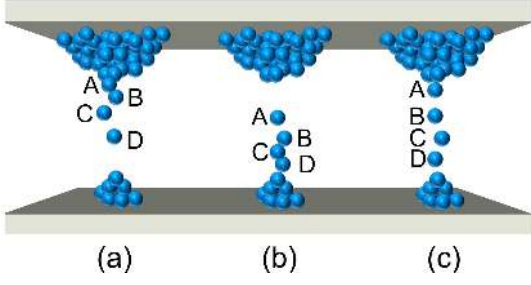
Fig. 8. Schematic picture of the fluctuation of the defect position in small CF, possibly contributing to the $I_C$-dependent variability in Fig. 7. The CF is assumed to consist of only four defects A, B, C and D in the gap region. For instance, defects can be located at the top side of the gap (a), at the bottom side of the gap (b) or be uniformly distributed (c), thus impacting the measured resistance for the same nominal size of the CF.
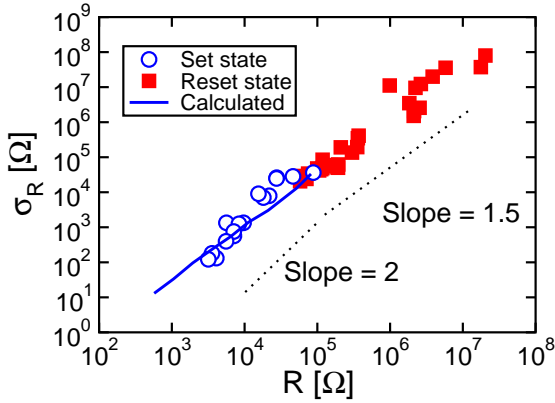


Fig. 9. Measured and calculated $\sigma_R$ as a function of $R$ for set and reset states. Different values of the set and reset state were obtained by varying $I_C$. Note the universal correlation with slope 1.5, consistent with Poisson statistics of Eq. (4).

## B. Reset state variability as a function of $I_C$

Fig. 9 shows the measured $\sigma_R$ as a function of $\mu_R$, for set and reset states. Data were collected from the switching statistics over 50 cycles, where different values of $R$ in the set and reset states were obtained by changing $I_C$. The curve shows a universal behavior with a slope of 1.5 for reset states and a higher slope around 2 for set states. The slope of 1.5 for the reset state is consistent with Poisson statistics, as can be analytically described in the following. Poole-Frenkel (PF) current in the reset state is proportional to the density of localized states which act as centers for thermally-activated emission of carriers. Assuming that injected defects all contribute to PF current, the reset-state resistance $R$ can thus be written as:

$$R = B \frac{e^{\frac{E_C}{kT}}}{A_{CF} n_D} = B e^{\frac{E_C}{kT}} \frac{\Delta}{N_D}, \qquad (3)$$

where $B$ is a pre-exponential constant, $A_{CF}$ is the CF cross section area, $E_C$ is the PF energy barrier controlling the activation energy for conduction in the reset state, $n_D$ is the defect density and $N_D$ is the defect number in the gap region of length $\Delta$, which controls $R$ in the reset state. Since $N_D$ is affected by Poisson fluctuations with spread $\sigma_{N_D} = N_D^{0.5}$, the
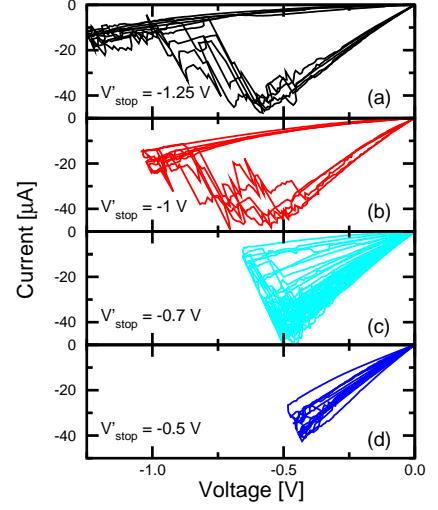


Fig. 10. Measured reset characteristics for decreasing maximum voltage, namely $V'_{stop}$ = -1.25 V (a), -1 V (b), -0.7 V (c) and -0.5 V (d). $V'_{stop}$ is the voltage across the 1T1R structure, which is slighty larger than the effective $V_{stop}$ in the figure. Variability in the reset transition affects the spread in the resistance distribution.
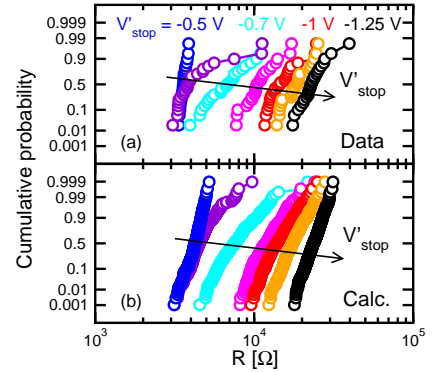


Fig. 11. Measured (a) and calculated (b) distributions of resistance for increasing $V'_{stop}$. A low $V'_{stop}$ is not able to trigger the reset operation, thus the relatively small spread of the set state is retained. For $V'_{stop} \approx V_{reset}$, the spread becomes large as a result of the reset variability. The distribution finally tightens for high $V'_{stop}$, reflecting the completion of the reset transition.

spread of the resistance can be obtained as [7]:

$$\sigma_R = \frac{R \sigma_{N_D}}{N_D} \propto R^{1.5}, \qquad (4)$$

The universal spread in Fig. 9 suggests that variability steeply increases with $R$ for both the set and reset state. Decreasing $I_C$ causes a resistance increase of both set and reset states, therefore reducing $I_C$ might result in a significant degradation of resistance distribution.

## C. Reset state variability as a function of $V_{stop}$

The reset state $R$ is not only controlled by $I_C$, but also by $V_{stop}$ dictating the maximum voltage along the reset sweep. Due to the gradual increase of $R$ along the reset transition, $V_{stop}$ must be maximized for a better $R$ window between set and reset states. We have studied the impact of $V_{stop}$ on $R$ variability by changing $V'_{stop}$, namely the maximum
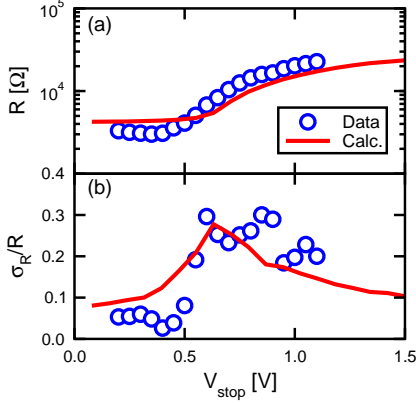
Fig. 12. Measured and calculated resistance (a) and relative spread $\sigma_R/R$ (b) as a function of $V'_{stop}$, obtained from the distributions of resistance in Fig. 11.

voltage across the 1T1R device in the reset operation ($V'_{stop}$ is slightly larger than $V_{stop}$ in Fig. 1b due to the voltage drop across the select MOSFET). For instance, Fig. 10a shows the measured reset characteristics for $V'_{stop}$ = -1.25 V over several cycles on the same device, which leads to the tight distribution of $R$ reported in Fig. 11a. Reducing $V'_{stop}$ to -1 V in Fig. 10b changes the distribution quite negligibly, however the resistance distribution significantly broadens for $V'_{stop}$ = -0.7 V, as shown by the $I$-$V$ curves in Fig. 10c and by the cumulative distribution of $R$ at variable $V'_{stop}$ in Fig. 11a. The variability increase is due to $V'_{stop}$ being located in the transition region of the $I$-$V$ curves, where discrete migration events induce resistance changes. Due to the random occurrence of the discrete reset events, the resistance achieved at $V'_{stop}$ also changes significantly from cycle to cycle. In this intermediate range of $V'_{stop}$, in fact, the reset process may be almost complete in some case, whereas in other cases the reset process is largely incomplete or still to be initiated. This large statistical spread is due to the large range of energy barriers in Fig. 5. Finally, for very low $V'_{stop}$ = -0.5 V, the reset transition has barely started in the device, therefore the resistance is relatively low, close to the initial value for the set state, and its distribution is also relatively narrow.

The $V'_{stop}$-dependent $R$ and its corresponding fluctuation were studied by the Monte Carlo model, as shown by simulation results for the $R$ distributions in Fig. 11b. The distributions are relatively tight for the full reset state at high $V'_{stop}$, then a tail gradually appears and the overall distribution increases its spread at decreasing $V'_{stop}$. Finally, a narrow $R$ distribution is achieved again at low $V'_{stop}$, corresponding to the set state. Fig. 12 summarizes the measured and calculated median $R$ (a) and the relative spread $\sigma_R/R$ (b) as a function of $V'_{stop}$. The median $R$ increases gradually with $V'_{stop}$, while the relative spread first steeply increases for $V_{stop} \approx V_{reset} \approx 0.5$ V, then gradually decreases as the distribution tightens again at high $V'_{stop}$. The calculated results agree well with the reported data, validating our Monte Carlo model for variability prediction. These results suggest that a relatively wide set/reset window can be achieved at high $V'_{stop}$, which is also beneficial to improve the distribution spread. On
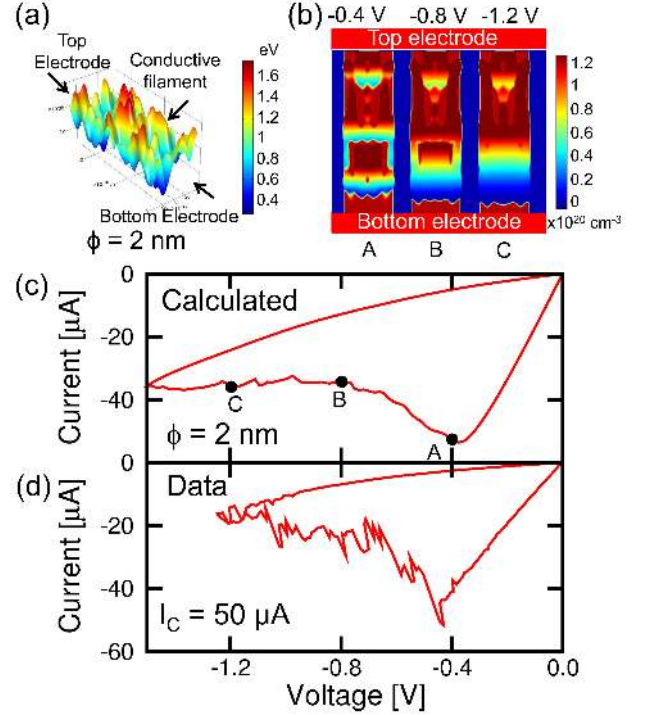


Fig. 13. Calculated energy landscape for ion migration (a), map of calculated defect concentration in the CF at bias points -0.4 V (A), -0.8 V (B), -1.2 V (C) for $\phi$ = 2 nm, calculated $I$-$V$ curve for the reset transition (c) and corresponding measured curve for a comparable $I_{reset}$ = 50 $\mu$A (d).

the other hand, a high $V'_{stop}$ was shown to lead to a degradation of both endurance [27] and retention [28], therefore a careful tradeoff between high resistance window and reliability should be considered for the choice of $V'_{stop}$ in the reset operation.

## VI. NUMERICAL MODEL

To gain a deeper insight into the reset mechanism, we extended the ionic drift-diffusion numerical model [17] to statistical switching fluctuations by a Monte Carlo approach. In this model, the ionic drift-diffusion flux [cm$^{-2}$s$^{-1}$] is given by:

$$\vec{j} = -D\vec{\nabla}n_D + \frac{qD}{kT}\vec{F}n_D, \tag{5}$$

where $n_D$ is the defects density [cm$^{-3}$], $q$ is the electron charge and $\vec{F}$ is the electric field. The ion diffusivity $D$ [cm$^2$s$^{-1}$] is modeled by the Arrhenius formula, namely:

$$D = D_0 e^{-\frac{E_A}{kT}}, \tag{6}$$

where $D_0$ is a pre-exponential factor [cm$^2$s$^{-1}$]. To introduce a statistical fluctuation from cycle to cycle in the model, a non-uniform distribution of $E_A$ was randomly generated within the CF region by an energy landscape approach [29]. In this approach, $E_A$ is assumed to randomly change with the position in the CF region, therefore resulting in strong fluctuations of ionic conductivity which leads to percolation effects. Fig. 13a shows the calculated map of $E_A$ for a CF with diameter $\phi$ = 2 nm. The local variation of $E_A$ reflects the disordered
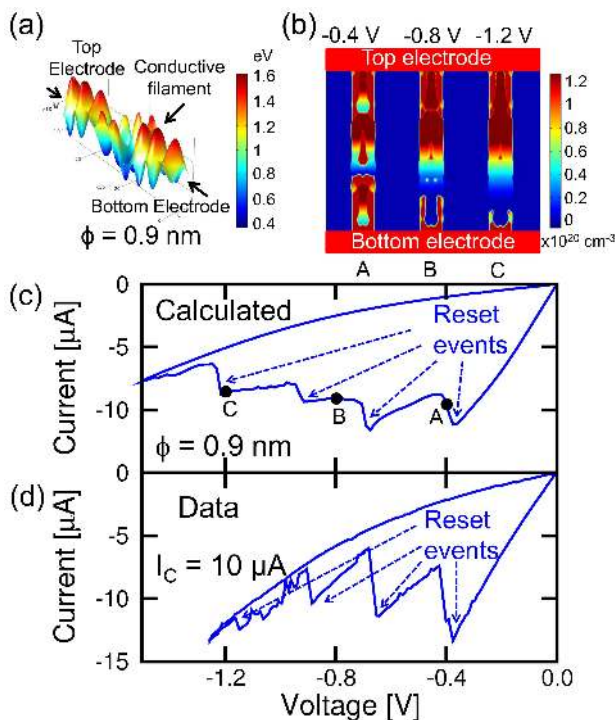
Fig. 14. Same as Fig. 13, but for $\phi$ = 0.9 nm and for an experimental reset current of $I_{reset}$ = 10 $\mu$A.

temperature, reach the value needed to induce migration over a critical $E_A$ barrier in the energy landscape. A typical $I$-$V$ curve in Fig. 14d also displays discrete reset events for small $I_C$, while discrete reset events are less visible in Fig. 13 due to averaging effects. These results also allow a physical interpretation of the sudden switching events in the measured $I$-$V$ curves as due to sudden migration of defect clusters in the non-uniform $E_A$ landscape.

## VII. CONCLUSIONS

The switching variability of $HfO_x$-based RRAM devices has been modeled by a Monte Carlo approach, which describes the discrete injection of defects. The model can capture the main trends of set and reset variability, including the $I_C$-dependence of the switching distribution for set and reset, and the $V'_{stop}$-dependence of the reset state distribution. A numerical model is finally proposed to provide a microscopic picture of random defect migration during the reset process. The Monte Carlo models allow to predict the statistical variation of resistance and other switching parameters for variable operating conditions.

## VIII. ACKNOWLEDGMENTS

## REFERENCES

[1] R. Waser and M. Aono, "Nanoionics-based resistive switching memories," *Nat. Mat.*, vol. 6, pp. 833–840, 2007.

[2] M. D. Pickett and R. S. Williams, "Sub-100 fJ and sub-nanosecond thermally driven threshold switching in niobium oxide crosspoint nanodevices," *Nanotechnology*, vol. 23, p. 215202, 2012.

[3] H. Y. Lee, P. S. Chen, T. Y. Wu, Y. S. Chen, C. C. Wang, P. J. Tzeng, C. H. Lin, F. Chen, C. H. Lien, and M.-J. Tsai, "Low power and high speed bipolar switching with a thin reactive Ti buffer layer in robust $HfO_2$ based RRAM," *IEDM Tech. Dig.*, pp. 1–4, 2008.

[4] F. Nardi, D. Ielmini, C. Cagli, S. Spiga, M. Fanciulli, L. Goux, and D. J. Wouters, "Control of filament size and reduction of reset current below 10 $\mu$a in NiO resistance switching memories," *Solid State Electronics*, vol. 58, pp. 42–47, 2011.

[5] X. Guan, S. Yu, and H.-S. Wong, "On the switching parameter variation of metal-oxide RRAM - Part I: Physical modeling and simulation methodology," *IEEE Trans. Electron Devices*, vol. 59, no. 4, pp. 1172–1182, 2012.

[6] J. Shin, J. Park, J. Lee, S. Park, S. Kim, W. Lee, I. Kim, D. Lee, and H. Hwang, "Effect of program/erase speed on switching uniformity in filament-type RRAM," *IEEE Electron Device Lett.*, vol. 32, no. 7, pp. 958–960, 2011.

[7] S. Balatti, S. Ambrogio, D. C. Gilmer, and D. Ielmini, "Set variability and failure induced by complementary switching in bipolar RRAM," *IEEE Electron Device Lett.*, vol. 34, no. 7, pp. 861–863, 2013.

[8] A. Fantini, L. Goux, R. Degraeve, D. J. Wouters, N. Raghavan, G. Kar, A. Belmonte, Y.-Y. Chen, B. Govoreanu, and M. Jurczak, "Intrinsic switching variability in $HfO_2$ RRAM," *International Memory Workshop IMW*, pp. 30–33, 2013.

[9] N. Raghavan, R. Degraeve, A. Fantini, L. Goux, D. J. Wouters, G. Groeseneken, and M. Jurczak, "Stochastic variability of vacancy filament configuration in ultra-thin dielectric RRAM and its impact on OFF-state reliability," *IEDM Tech. Dig.*, pp. 554–557, 2013.

[10] R. Degraeve, A. Fantini, N. Raghavan, Y. Y. Chen, L. Goux, S. Clima, S. Cosemans, B. Govoreanu, D. J. Wouters, P. Roussel, G. S. Kar, G. Groeseneken, and M. Jurczak, "Modeling RRAM set/reset statistics resulting in guidelines for optimized operation," *Symp. VLSI Tech. Dig.*, pp. T98–T99, 2013.

[11] D. Ielmini, F. Nardi, and C. Cagli, "Resistance-dependent amplitude of random telegraph-signal noise in resistive switching memories," *Appl. Phys. Lett.*, vol. 96, no. 5, p. 053503, 2010.

structure and mechanical stress distribution in the gap region, where structural defects, such as vacancies and dislocations, can provide localized states and/or paths for ion hopping. Fig. 13b shows the evolution of the defect concentration during a negative voltage sweep, while Fig. 13c shows the corresponding $I$-$V$ curve for the reset transition. The concentration is mapped at three different states A, B and C, corresponding to V = -0.4, -0.8 and -1.2 V. As ionized defects migrate toward the negatively-biased top electrode, the gap length increases. Due to the non-uniform distribution of $E_A$, migration takes place over percolation paths with the lowest $E_A$, resulting in irregular boundaries of the depleted gap. Fig. 13d shows the experimental $I$-$V$ curve for a similar $I_{reset}$ of about 50 $\mu$A. Note that the experimental current both displays increasing and decreasing steps. This might be explained by the transfer of defects from the bottom reservoir to the top reservoir, where a defect stopping in an intermediate position within the gap might temporarily increase the conductivity [17]. As the defect completes the transition, the conductivity decreases again to an even higher value according to the reset process.

To highlight the size dependence of switching fluctuations, Fig. 14 shows simulation results for the energy landscape (a), the defect concentration map (b), and the calculated reset characteristic (c) for a CF diameter of 0.9 nm. Fig. 14d shows the measured $I$-$V$ curve for a comparable $I_{reset}$ of about 10 $\mu$A. The smaller CF results in a smaller number of percolation paths for defect migration, which makes discrete reset events more visible in the $I$-$V$ curve of Fig. 14c. Each discrete reset event corresponds to the sudden increase of the gap length as the driving forces for migration, namely electric field and

[12] D. Veksler, G. Bersuker, L. Vandelli, A. Padovani, L. Larcher, A. Mu-
raviev, B. Chakrabarti, E. Vogel, D. C. Gilmer, and P. D. Kirsch,
"Random telegraph noise (RTN) in scaled RRAM devices," *International
Reliability Physics Symposium (IRPS)*, pp. 101–104, 2013.

[13] N. Raghavan, R. Degraeve, A. Fantini, L. Goux, S. Strangio, B. Gov-
oreanu, D. J. Wouters, G. Groeseneken, and M. Jurczak, "Microscopic
origin of random telegraph noise fluctuations in aggressively scaled
RRAM and its impact on read disturb variability," *International Re-
liability Physics Symposium (IRPS)*, pp. 5E.3.1–5E.3.7, 2013.

[14] F. T. Chen, H.-Y. Lee, Y.-S. Chen, S. Z. Rahaman, C.-H. Tsai, K.-
H. Tsai, T.-Y. Wu, W.-S. Chen, P.-Y. Gu, Y.-D. Lin, S.-S. Sheu, M.-
J. Tsai, L.-H. Lee, T.-K. Ku, and P.-S. Chen, "Resistance instabilities
in a filament-based resistive memory," *International Reliability Physics
Symposium (IRPS)*, pp. 5E.1.1–5E.1.7, 2013.

[15] K. Prall, N. Ramaswamy, W. Kinney, K. Holtzclaw, X. Che, J. Strand,
and R. Bez, "An update on emerging memory: Progress to 2Xnm,"
*International Memory Workshop IMW*, pp. 1–5, 2012.

[16] S. Ambrogio, S. Balatti, A. Cubeta, A. Calderoni, N. Ramaswamy, and
D. Ielmini, "Understanding switching variability and random telegraph
noise in resistive RAM," *IEDM Tech. Dig.*, pp. 782–785, 2013.

[17] S. Larentis, F. Nardi, S. Balatti, D. C. Gilmer, and D. Ielmini, "Resistive
switching by voltage-driven ion migration in bipolar RRAM - Part II:
Modeling," *IEEE Trans. Electron Devices*, vol. 59, no. 9, pp. 2468–2475,
2012.

[18] S. Ambrogio, S. Balatti, A. Cubeta, A. Calderoni, N. Ramaswamy,
and D. Ielmini, "Statistical fluctuations in $HfO_x$ resistive-switching
memory (RRAM): Part II - Random telegraph noise," *IEEE Trans.
Electron Devices*, vol. submitted, 2014.

[19] F. Nardi, S. Larentis, S. Balatti, D. C. Gilmer, and D. Ielmini, "Resistive
switching by voltage-driven ion migration in bipolar RRAM - Part I:
Experimental study," *IEEE Trans. Electron Devices*, vol. 59, no. 9,
pp. 2461–2467, 2012.

[20] S. Yu, Y. Wu, and H.-S. P. Wong, "Investigating the switching dynamics
and multilevel capability of bipolar metal oxide resistive switching
memory," *Appl. Phys. Lett.*, vol. 98, no. 10, p. 103514, 2011.

[21] K. Kinoshita, K. Tsunoda, Y. Sato, H. Noshiro, S. Yagaki, M. Aoki,
and Y. Sugiyama, "Reduction in the reset current in a resistive random
access memory consisting of $NiO_x$ brought about by reducing a parasitic
capacitance," *Appl. Phys. Lett.*, vol. 93, no. 3, p. 033506, 2008.

[22] U. Russo, D. Kamalanathan, D. Ielmini, A. L. Lacaita, and M. N. Koz-
icki, "Study of multilevel programming in programmable metallization
cell (PMC) memory," *IEEE Trans. Electron Devices*, vol. 56, no. 5,
pp. 1040–1047, 2009.

[23] S. Yu and H.-S. P. Wong, "Compact modeling of conducting-bridge
random-access memory (CBRAM)," *IEEE Trans. Electron Devices*,
vol. 58, no. 5, pp. 1352–1360, 2011.

[24] S. Balatti, S. Ambrogio, D. Ielmini, and D. C. Gilmer, "Variability and
failure of set process in HfO$_2$ RRAM," *International Memory Workshop
IMW*, pp. 38–41, 2013.

[25] D. Ielmini, "Modeling the universal set/reset characteristics of bipolar
RRAM by field- and temperature-driven filament growth," *IEEE Trans.
Electron Devices*, vol. 58, no. 12, pp. 4309–4317, 2011.

[26] D. Ielmini, F. Nardi, and C. Cagli, "Universal reset characteristics
of unipolar and bipolar metal-oxide RRAM," *IEEE Trans. Electron
Devices*, vol. 58, no. 10, pp. 3246–3253, 2011.

[27] Y. Y. Chen, B. Govoreanu, L. Goux, R. Degraeve, A. Fantini, G. S.
Kar, D. J. Wouters, G. Groeseneken, J. A. Kittl, M. Jurczak, and
L. Altimime, "Balancing SET/RESET pulse for $> 10^{10}$ endurance in
HfO$_2$/Hf 1T1R bipolar RRAM," *IEEE Trans. Electron Devices*, vol. 59,
no. 12, pp. 3243–3249, 2012.

[28] S. Muraoka, T. Ninomiya, Z. Wei, K. Katayama, R. Yasuhara, and
T. Takagi, "Comprehensive understanding of conductive filament char-
acteristics and retention properties for highly reliable ReRAM," *Symp.
VLSI Tech. Dig*, pp. 62–63, 2013.

[29] M. Rizzi, M. Ferro, P. Fantini, and D. Ielmini, "Energy landscape model
of conduction and phase transition in phase change memories," *IEEE
Trans. Electron Devices*, vol. 60, no. 11, pp. 3618–3624, 2013.